A Ka-band tunable direct-conversion correlation reflectometer for NSTX[a)]

S. Kubota,[1,b)] W. A. Peebles,[1] X. V. Nguyen,[1] N. A. Crocker,[1] A. L. Roquemore,[2] T. Holoman,[2] L. Guttadora,[2] and R. Kaita[2]
[1]*Department of Physics and Astronomy, University of California, Los Angeles, California 90095, USA*
[2]*Princeton Plasma Physics Laboratory, Princeton, New Jersey 08543, USA*

(Presented 18 May 2010; received 16 May 2010; accepted 2 August 2010; published online 21 October 2010)

The recent availability of broadband microwave quadrature mixers in the Ka-band (28–40 GHz) of frequencies has allowed the fabrication of low-cost direct-conversion detection circuits for use in the variable-frequency correlation reflectometer on the National Spherical Torus eXperiment (NSTX). The quadrature receiver in this case can be implemented as a simple homodyne circuit, without the complication of a single-sideband modulator or a feedforward tracking circuit present in more typical designs. A pair of direct-conversion receivers is coupled with broadband microwave voltage-controlled oscillators to construct a flexible dual-channel radar system with a fast frequency settling time of ~160 μs. A detailed description of the design and a full characterization of the hardware are provided. Examples of turbulence measurements from radial and poloidal correlation reflectometry on NSTX using a poloidal array of antennas (oriented normal to the magnetic flux surfaces for conventional reflectometry) are presented. © *2010 American Institute of Physics.*
[doi:10.1063/1.3490024]

I. INTRODUCTION

In magnetic fusion devices, the measurement and characterization of turbulence properties such as correlation lengths, fluctuation level, and frequency- and wavenumber-spectra are key ingredients for studying microinstabilities and their associated particle, energy, and momentum transport.[1] With regards to electron density fluctuations, reflectometry has played an important role as one the few diagnostics capable of direct internal measurements with the required time and spatial resolutions for extracting the properties of low-k (Ref. 2) and intermediate-k (Ref. 3) turbulence.

Reflectometry is a radar-based diagnostics that launches a microwave beam into the plasma at a frequency f_0 and detects the reflected beam from the cutoff layer. The cutoff layer can be either a sole function of the electron density n_e in the case of O-mode polarization [$f_0=f_{pe}(n_e)$], or a function of both the electron density and the magnetic field strength B in the case of X-mode polarization [right-hand cutoff $f_0=f_{rhc}(n_e,B)$]. Density fluctuations near the cutoff layer and along the beam path produce phase and amplitude (or complex amplitude) fluctuations in the return beam. The beam orientation is configured to be roughly normal to the cutoff surface for low-k (conventional reflectometry) measurements, or at an oblique angle for intermediate-k (Doppler backscattering) measurements. Here we concentrate exclusively on the conventional reflectometry configuration.

In correlation reflectometry, two or more microwave beams are launched and received simultaneously. They can be either collinear for radial correlation measurements or azimuthally distributed for poloidal or toroidal correlation measurements. In either configuration, low-k turbulence quantities such as the fluctuation level, correlation length, and flow velocity may be inferred. Correlation reflectometers have been used for turbulence measurements on a variety of devices, e.g., ATF,[4] DIII-D,[5] CCT,[6] LAPD,[7] JT- 60U,[8] National Spherical Torus eXperiment (NSTX),[9] T-10,[10] and TEXTOR.[11] For a single tunable-frequency channel in the Ka-band, quadrature detection typically requires heterodyne circuitry. One method for generating the intermediate frequency uses a single voltage-controlled oscillator (VCO) combined with a single side-band modulator, while a second method utilizes a pair of VCOs with a feedforward tracking circuit. In either case, the required hardware can become complex and costly when multiple channels become necessary. On the other hand, the recent availability of relatively low-cost direct-conversion quadrature mixers in the Ka-band allows one to substitute heterodyne detection with homodyne detection. The advantage here is the simplicity of the homodyne circuit, which requires only a single VCO and a single mixer.

This article describes the two-channel tunable Ka-band (28–40 GHz) correlation reflectometer, constructed for the NSTX,[12] utilizing direct-conversion mixers. The broadband homodyne quadrature technique comes with its own set of difficulties, e.g., large local oscillator power and conversion loss, as well as frequency-dependent dc offset levels and mixer imbalances. A detailed description of the microwave circuit and techniques used to overcome these issues is included. Finally, preliminary examples of radial and poloidal correlation measurements are presented.

[a)]Contributed paper, published as part of the Proceedings of the 18th Topical Conference on High-Temperature Plasma Diagnostics, Wildwood, New Jersey, May 2010.
[b)]Electronic mail: skubota@ucla.edu.

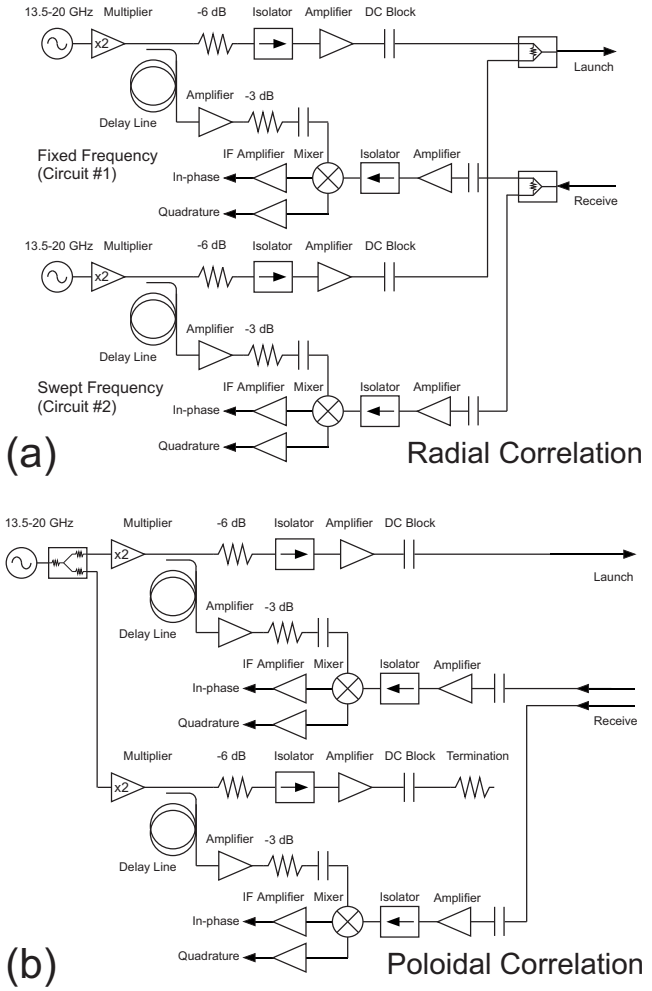

FIG. 1. Circuit diagrams of (a) the 28–40 GHz correlation reflectometer and (b) the 50 GHz quadrature reflectometer.

II. DIAGNOSTIC DESCRIPTION

The correlation reflectometer consists of two identical tunable-frequency reflectometer channels using direct-conversion (or homodyne quadrature detection). Transceiver circuits for radial and poloidal correlation measurements are shown in Figs. 1(a) and 1(b), respectively. Coaxial components are used throughout and the transceiver is housed in an aluminum shield box next to the machine. The microwave source is a 13.5–20 GHz hyperabrupt varactor-tuned oscillator (HTO) used in conjunction with an active 2× frequency multiplier (Marki A-2050) to obtain the final frequency range of 27–40 GHz. The tuning voltage (V_t) of the HTO is controlled by an Agilent 33220A arbitrary waveform generator (AWG) used with a 4× voltage amplifier for a final output in the range 0–20 V. Wilkinson dividers are used to combine or split the launched or reflected power in the radial correlation system. The launch power after the final amplifier stage ranges from 18 to 15 dBm per channel. Isolators on the output port eliminate reflection from the vacuum window.

The V_t amplifier design has been documented elsewhere.[13] In order to reduce the phase noise of the oscillator, the V_t amplifier output is heavily low-pass filtered with a −3 dB cutoff at 10 kHz. This reduces switching noise from the AWG output as well as pickup through the cables. The system is designed to be stepped relatively quickly and this bandwidth offers a settling time of ~160 μs.

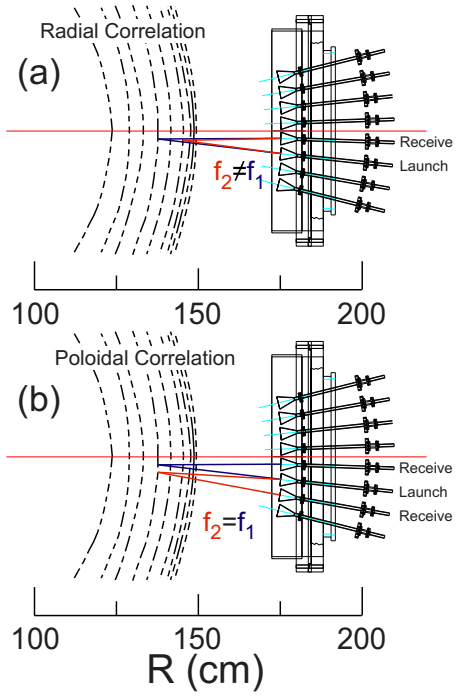

FIG. 2. (Color online) Poloidal Q-band antenna array showing launch and receive antenna geometries for (a) radial and (b) poloidal correlation measurements.

The transmission lines between the shield box and the vacuum vessel interface use low-loss coaxial cable. The instrument rack housing the microwave hardware lies close to the machine and requires a roundtrip cable length of ~9 ft (loss of ~6–7 dB). The total roundtrip loss including the transmission line to the machine and the path inside the vacuum vessel is ~25–30 dB. An amplifier is used at the end of the path to boost the radio frequency (rf) input signal to the mixer. The local oscillator (LO) signal to the mixer has a 14 ft coaxial delay line to offset the external transmission line path. This reduces the effects of phase noise from the oscillator. An amplifier is used at the end of the delay line both to provide the proper LO power to the mixer as well as to balance the attenuation characteristics of the coaxial cable. This is necessary for proper mixer biasing across the entire frequency band.

The mixer is a 26–40 GHz image rejection (I/Q) mixer (Miteq IR2640NI7Q), which has a conversion loss of ~9 dB but requires a large LO power of ~17 dBm. LO to rf port isolation in this case becomes an issue and the isolator on the receive port eliminates additional reflections from the vacuum window and plasma. Another important figure of merit is the relatively low dc offset at this LO power level (≲10 mV), since this lowers the 1 dB compression point for the rf power level (by ≲4 dB). The microwave amplifier on the receive path elevates the mixer rf input power to the appropriate level.

Figures 2(a) and 2(b) show the poloidal horn array used by the reflectometer located on a midplane port for either radial correlation or poloidal correlation measurements, respectively. Each channel utilizes a pair of circular launch and

receive horns, oriented roughly normal to the magnetic flux surfaces. Each horn assembly consists of a circular waveguide section followed by a rotary joint, a circular-to-rectangular waveguide transition, and a coaxial-to-waveguide adapter. The polarization direction is set by the orientation of the coaxial-to-waveguide adapter and is varied by rotating the rotary joint. The lower limit of the scannable frequency range is limited to 27.7 GHz by the cutoff of the circular waveguide; during experiments a range of 28.5–40 GHz is used. Transmission through each 0.006 in. mica window is better than 80%. The −3 dB full beamwidth over this frequency range is 17°–12°. A detailed description of the vacuum vessel interface is given elsewhere.[14]

The data acquisition and control hardware is housed in an instrument rack ~15 ft distant from the microwave hardware and consists of PC-based data acquisition cards and rackmounted AWGs. The AWGs are connected to the computer using GPIB and are loaded with a programmed waveform prior to the discharge. An NI PCI-6602 counter/timer cards provide a common clock for the data acquisition cards and a repetitive trigger for the AWGs, as well as for other supporting diagnostics.

III. SYSTEM CHARACTERIZATION AND PERFORMANCE

Documentation of the 26–40 GHz I/Q mixer characteristics are critical for proper operation of this diagnostic. For real mixers, the in-phase (I) output V_I and quadrature-phase (Q) output V_Q have dc offsets $V_{I,DC}$ and $V_{Q,DC}$, an amplitude imbalance ϵ, and a phase imbalance ϕ_0 defined by

$$V_I = (1+\epsilon)A\cos\phi + V_{I,dc} = (1+\epsilon)\bar{V}_I + V_{I,dc}, \quad (1)$$

$$V_Q = A\sin(\phi+\phi_0) + V_{Q,dc} = \bar{V}_Q\cos\phi_0 + \bar{V}_I\sin\phi_0 + V_{Q,dc}, \quad (2)$$

where A and ϕ are the true amplitude and phase. Knowing $V_{I,dc}$, $V_{Q,dc}$, ϵ, and ϕ_0, the signals can be corrected to allow simple calculation of $A=\sqrt{\bar{V}_I^2+\bar{V}_Q^2}$ and $\phi=\arctan(\bar{V}_I,\bar{V}_Q)$. Figure 3 plots the results of a calibration scan where the tuning voltage is finely stepped. The launch and receive ports are either (1) terminated to generate the dc offsets or (2) short-circuited to generate the I and Q fringes used to calculate the imbalances. The dc offsets limit the dynamic range of the mixer; a useful figure of merit is the ratio $\eta=(V_{-1\ dB}-V_{dc})/V_{-1\ dB}$, where $V_{-1\ dB}$ is the IF signal amplitude at the −1 dB compression point and V_{dc} is the dc offset ($\eta=0$ for $V_{dc}=V_{-1\ dB}$, $\eta=1$ for $V_{dc}=0$). In our case η_{min} ~0.5 and the rms amplitude for the corrected signals during a typical plasma shot is ~1–2 V.

For broadband HTOs, the largest source of phase noise is typically due to tuning voltage noise; for tunable-frequency systems this means that there is a tradeoff between low phase noise and fast response to a frequency step. Figure 4 shows a quadrant of the I and Q signal outputs during a plasma discharge where the launch and receive cables have been short-circuited, while the inset shows a plot of the receiver phase spectrum. With the 10 kHz filter on the V_t amplifier output, the system achieves an rms of ~0.3° (rms phase fluctuations from a typical plasma target are ~1–2 rad). The peaks at harmonics of 10 kHz are due to intrinsic switching noise on the AWG output.

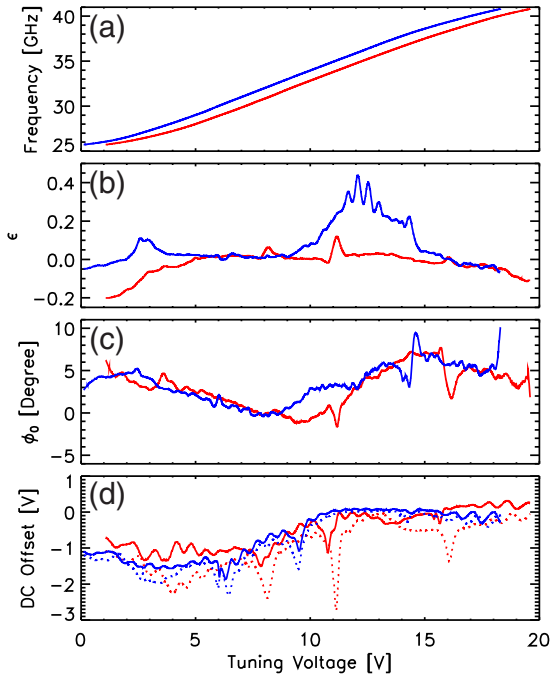

FIG. 3. (Color online) (a) Microwave frequency, (b) amplitude imbalance ϵ, (c) phase imbalance ϕ_0, and (d) dc offset (IF amplifier output) as a function of the tuning voltage. Here, blue (dark) and red (light) denote channels 1 and 2, respectively. In (d) the in-phase signal is shown by the solid curve while the quadrature signal is shown by the dashed curve.

IV. EXPERIMENTAL RESULTS

Figure 5 shows an example of a radial correlation measurement in the core a low density NSTX *L*-mode discharge using the antenna geometry shown in Fig. 1(a); here CH1 is stepped in frequency and CH2 remains fixed [Fig. 5(a)]. Figure 5(b) shows the absolute value of correlation coefficient

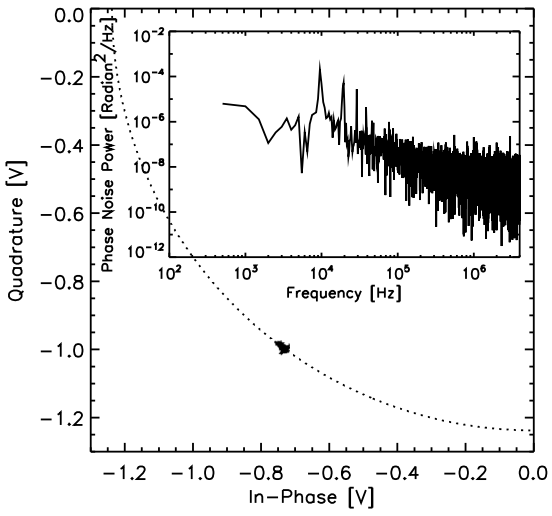

FIG. 4. Lower left quadrant of phasor diagram for in-phase and quadrature signals at 35 GHz for a 2 ms interval during a discharge where the launch and receive cables have been short-circuited. Inset shows the power spectrum of the phase noise (rms of 0.3°).

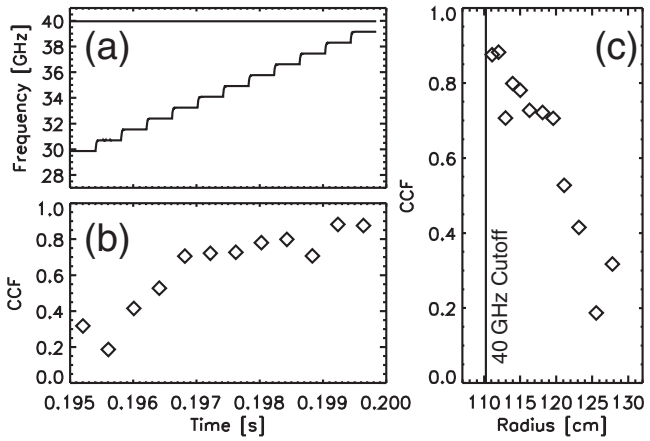

FIG. 5. Example of radial correlation measurement showing (a) the launched frequency versus time (CH1 is stepped, CH2 is fixed), (b) the CCF vs time, and (c) the CCF as a function of major radius.

function (CCF) between the two channels using the complex amplitude signal $\bar{V}_I(t)+i\bar{V}_Q(t)$, while Fig. 5(c) shows the same data plotted as a function of the major radius. Estimates of the actual density turbulence correlation length will require further analysis with full-wave simulations.[15]

Poloidal correlation measurements (Fig. 6) were made using the antenna geometry shown in Fig. 1(b) near the plasma edge during H-mode. Figures 6(b) and 6(c) show the coherence and cross-phase ϕ_{12} between the phase signals from the two channels at $f=33.1$ GHz. The velocities in Fig. 6(d) are estimated as $v=L/\tau$, where $\tau=d\phi_{12}/d\omega$ is the propagation time between the reflection points of the two channels (distance L apart). Here we assumed only poloidal flow with frozen fluctuations. Core poloidal correlation measurements will require the evaluation of geometric effects,[2,16] e.g., 2D diffraction effects due to beam propagation and asymmetries in the orientation of the horn pairs with respect to the cutoff surface.

Further analysis of the radial and poloidal correlation configurations on NSTX using a 2D full-wave code will be presented in a future paper.

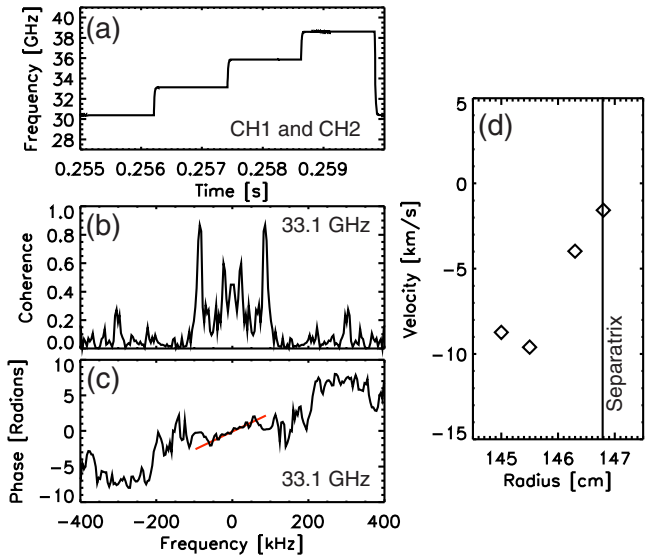

FIG. 6. (Color online) Example of poloidal correlation measurements showing (a) the launched frequency vs time, [(b) and (c)] the coherence and cross-phase for $f=33.1$ GHz (second frequency step), and (d) the poloidal velocity from the four frequency steps.

ACKNOWLEDGMENTS

This work is supported by U.S. DOE Contract Nos. DE-FG02-99ER54527 and DE-AC02- 09CH11466.

[1] G. R. Tynan, A. Fujisawa, and G. McKee, Plasma Phys. Controlled Fusion **51**, 113001 (2009).
[2] R. Nazikian, G. J. Kramer, and E. J. Valeo, Phys. Plasmas **8**, 1840 (2001).
[3] G. D. Conway, Plasma Phys. Controlled Fusion **50**, 124026 (2008).
[4] G. R. Hanson, J. B. Wilgen, E. Anabitarte, J. D. Bell, J. H. Harris, J. L. Dunlap, and C. E. Thomas, Rev. Sci. Instrum. **61**, 3049 (1990).
[5] T. L. Rhodes, J.-N. Leboeuf, R. D. Sydora, R. J. Groebner, E. J. Doyle, G. R. McKee, W. A. Peebles, C. L. Rettig, L. Zeng, and G. Wang, Phys. Plasmas **9**, 2141 (2002).
[6] T. L. Rhodes, W. A. Peebles, E. J. Doyle, P. Pribyl, M. Gilmore, R. A. Moyer, and R. D. Lehmer, Plasma Phys. Controlled Fusion **40**, 493 (1998).
[7] M. A. Gilmore, W. A. Peebles, and X. V. Nguyen, Plasma Phys. Controlled Fusion **42**, 655 (2000).
[8] N. Oyama and K. Shinohara, Rev. Sci. Instrum. **73**, 1169 (2002).
[9] M. A. Gilmore, W. A. Peebles, S. Kubota, X. V. Nguyen, and A. Ejiri, Rev. Sci. Instrum. **74**, 1469 (2003).
[10] V. A. Vershkov, V. V. Drevel, and S. V. Soldatov, Rev. Sci. Instrum. **70**, 1700 (1999).
[11] A. Krämer-Flecken, V. Drevel, S. Soldatov, A. Rogister, V. Vershkov, and the TEXTOR Team, Nucl. Fusion **44**, 1143 (2004).
[12] M. Ono, S. M. Kaye, Y.-K. M. Peng, G. Barnes, W. Blanchard, M. D. Carter, J. Chrzanowski, L. Dudek, R. Ewig, D. Gates, R. E. Hatcher, T. Jarboe, S. C. Jardin, D. Johnson, R. Kaita, M. Kalish, C. E. Kessel, H. W. Kugel, R. Maingi, R. Majeski, J. Manickam, B. McCormack, J. Menard, D. Mueller, B. A. Nelson, B. E. Nelson, C. Neumeyer, G. Oliaro, F. Paoletti, R. Parsells, E. Perry, N. Pomphrey, S. Ramakrishnan, R. Raman, G. Rewoldt, J. Robinson, A. L. Roquemore, P. Ryan, S. Sabbagh, D. Swain, E. J. Synakowski, M. Viola, M. Williams, J. R. Wilson, and NSTX Team, Nucl. Fusion **40**, 557 (2000).
[13] S. Kubota, W. A. Peebles, X. V. Nguyen, N. A. Crocker, and A. L. Roquemore, Rev. Sci. Instrum. **77**, 10E926 (2006).
[14] S. Kubota, X. V. Nguyen, W. A. Peebles, L. Zeng, E. J. Doyle, and A. L. Roquemore, Rev. Sci. Instrum. **72**, 348 (2001).
[15] G. J. Kramer, R. Nazikian, and E. J. Valeo, Rev. Sci. Instrum. **74**, 1421 (2003).
[16] A. Ejiri, T. Yamada, Y. Adachi, O. Watanabe, and Y. Takase, Plasma Phys. Controlled Fusion **50**, 065003 (2008).